Brightness and duration of x-ray line sources irradiated with intense 0.53-μm laser light at 60 and 120 ps pulse width

D. W. Phillion
Lawrence Livermore National Laboratory, University of California, P.O. Box 808, Livermore, California 94550

C. J. Hailey
KMS Fusion, Inc., Ann Arbor, Michigan 48104

(Received 14 March 1986; revised manuscript received 11 June 1986)

Short, bright pulses of x-ray line emission are needed for flash radiography of laser-fusion targets. The experiments described here were carried out with the nominal laser pulse lengths of 60 and 120 ps. The $M \rightarrow L$ spectra were for Y (2.00–2.35 keV), Pd (2.95–3.46 keV), and Cs (4.43–5.15 keV), and the $L \rightarrow K$ spectra were for Cl (2.790 keV), Ti (4.749 keV), Mn (6.180 keV), and Ni (7.804 keV). The $L \rightarrow K$ energies are for the $1s2p\ ^1P_1 \rightarrow 1s^2\ ^1S_0$ transition. Both the duration and the absolute brightness of the x-ray line emission were measured. Even at 60 ps, the x-ray flashes from Y, Pd, and Ti were all bright and of duration comparable to or shorter than the laser pulse length. In particular, the Pd $M \rightarrow L$ lines were as bright as 2×10^{12} photons/j sr and the Ti $L \rightarrow K$ lines as bright as 5×10^{10} photons/j sr.

I. INTRODUCTION

Experiments performed with the KMS Chroma laser at 0.53 μm have succeeded in producing bright 50-ps (or shorter) x-ray flashes at 2.00–2.36 keV (yttrium $M \rightarrow L$ transitions), 2.95–3.46 keV (palladium $M \rightarrow L$ transitions), and 4.75 keV (titanium $1s2p$-$1s^2$ transitions). Scaling arguments based upon an exact two-parameter transformation group of the hydrodynamic equations suggest that, in light of these experimental results, it may be possible to generate 10–20-ps x-ray flashes at energies as high as 6 keV with intense 0.26-μm laser light. The hydrodynamic equations upon which the transformation group is based assume flux-limited classical electron heat transport and an ideal-gas equation of state. Radiation transport and cooling are neglected. Experiments by Yaakobi *et al.*[1] have shown that for a 0.35-μm irradiation wavelength, some x-ray lines can be as much as an order of magnitude brighter than for 1.06-μm irradiation. Matthews *et al.*[2] also noted substantially higher conversion efficiency at shorter wavelengths for several lines.

The measurements on the conversion efficiency ξ_x and the x-ray duration τ_x are presented first. We discuss the physics in an effort to understand the trends that were observed and then present the two-parameter transformation group. The Appendix gives the experimental details, including the film and crystal calibrations that were used.

II. EXPERIMENTAL RESULTS

Table I summarizes the experiments, which were at the nominal laser pulse lengths of 60 and 120 ps and at the laser wavelength of 0.53 μm. The targets were thick disks irradiated by a converging beam focused by an $f/1.8$ par-

TABLE I. Summary of the KMS x-ray flash backlighter characterization experiments.

Materials and x-ray lines	For the experiment with maximum ξ_x: ξ_x [photons/(joule sphere)]	Laser intensity (W/cm^2)	Laser FWHM (ps)	X-ray FWHM (ps)	Range of the x-ray FWHM for all experiments (ps)
At 120-ps FWHM pulse length:					
Cl K (2.79 keV $^1P_1$ Heα)	105×10^{11}	8.0×10^{14}	124	126	82–139
Pd L (2.95–3.46 keV neonlike)	380×10^{11}	$0.6\text{–}1.6 \times 10^{15}$	108	157	64–157
Ti K (4.75 keV $^1P_1$ Heα)	13×10^{11}	1.6×10^{15}	102	115	80–117
Cs L (4.43–5.15 keV neonlike)	16×10^{11}	$2.3\text{–}4.6 \times 10^{15}$	115	110	83–110
Mn K (6.18 keV $^1P_1$ Heα)	3.4×10^{11}	6.0×10^{14}	130	121	98–127
Ni K (7.80 keV $^1P_1$ Heα)	0.85×10^{11}	$1.3\text{–}2.5 \times 10^{16}$	104	103	87–100
At 60-ps FWHM pulse length:					
Yt L (2.00–2.36 keV neonlike)	240×10^{11}	1.6×10^{15}	~60	67	57–67
Pd L (2.95–3.46 keV neonlike)	190×10^{11}	$0.9\text{–}1.6 \times 10^{15}$	80	60	51–66
Ti K (4.75 keV $^1P_1$ Heα)	6.1×10^{11}	1.1×10^{16}	57	49	48–50
Mn K (6.18 keV $^1P_1$ Heα)	1.6×10^{11}	$0.9\text{–}1.8 \times 10^{16}$	70	57	56–57

TABLE II. Summary of the $M \rightarrow L$ emission-band experiments at 0.53 μm.

Element	FWHM laser pulse width (ps)	Laser energy (J)	FWHM spot diam from the x-ray pinhole camera (μm)	Focal offset (μm)	Laser intensity (W/cm^2)	Conversion efficiency, ξ_x [photons/(joule sphere)]	X-ray FWHM (ps)
Yttrium	~60	17.9	133 (sat.)	-200	0.5-1.1 x 10^{16}	1.9 x 10^{13}	57
	~60	12.2	126	-360	1.6 x 10^{15}	2.4 x 10^{13}	67
Palladium	80	14.4	84 (sat.)	0	0.9-1.6 x 10^{16}	191 x 10^{11}	66
	79	13.0	64 (sat.)	0	0.8-1.5 x 10^{16}	169 x 10^{11}	65
	64	3.6	40	0	4.5 x 10^{15}	142 x 10^{11}	—
	83	16.2	130 (sat.)	-200	2.7-9.2 x 10^{15}	143 x 10^{11}	67
	~70	1.6	35	0	2.4 x 10^{15}	70 x 10^{11}	—
	~70	11.9	165	-360	8.0 x 10^{14}	93 x 10^{11}	59
	63	21.1	284	-580	5.3 x 10^{14}	135 x 10^{11}	—
	65	19.0	281	-580	4.7 x 10^{14}	230 x 10^{11}[a]	59
	68	7.6	173	-360	4.8 x 10^{14}	134 x 10^{11}	51
	65	17.4	328	-770	3.2 x 10^{14}	68 x 10^{11}	55
	104	42.8	118 (sat.)	0	2.0-3.8 x 10^{16}	156 x 10^{11}	118
	115	37.5	105 (sat.)	0	1.6-3.0 x 10^{16}	204 x 10^{11}	131
	118	33.1	140 (sat.)	-200	4.2-9.9 x 10^{15}	204 x 10^{11}	118
	117	45.7	200 (sat.)	-360	1.8-5.4 x 10^{15}	265 x 10^{11}	151
	~120	36.2	168 (sat.)	-360	1.4-4.2 x 10^{15}	232 x 10^{11}	140
	108	39.6	247 (sat.)	-580	0.6-1.6 x 10^{15}	378 x 10^{11}	157
	114	34.6	287	-920	4.7 x 10^{14}	204 x 10^{11}	131
	116	3.0	99	-360	3.4 x 10^{14}	110 x 10^{11}	68
	116	8.5	266	-810	1.3 x 10^{14}	40 x 10^{11}	64
Cesium	~120	26.1	97 (sat.)	0	1.1-2.0 x 10^{16}	11 x 10^{11}	—
	~120	24.1	124 (sat.)	-200	3.0-7.1 x 10^{15}	—	90
	115	37.9	190 (sat.)	-360	2.3-4.6 x 10^{15}	16 x 10^{11}	110
	91	32.9	269 (sat.)	-580	0.6-1.6 x 10^{15}	12 x 10^{11}	83

[a] Obtained from ratio of time-resolved data. Time-integrated data were not acquired.

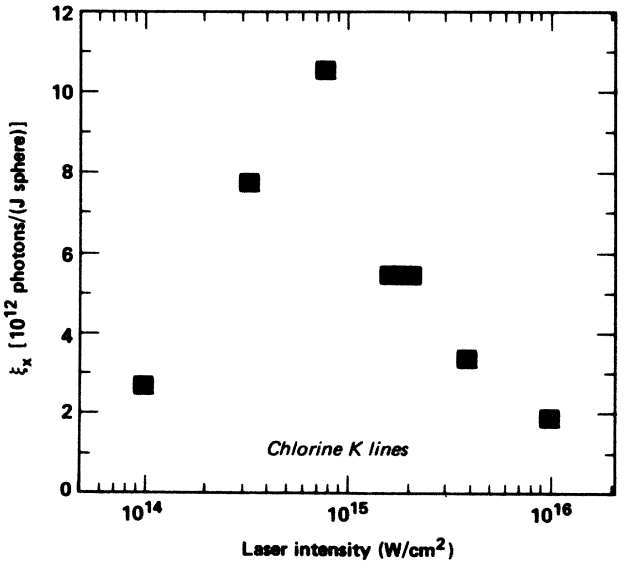

FIG. 1. Conversion efficiency vs laser intensity for He-like and Li-like chlorine $2p \rightarrow 1s$ transitions. Neither the $K\alpha$ nor the $H\alpha$ lines were summed over. The energy limits on the integration were typically 2.725—2.805 keV.

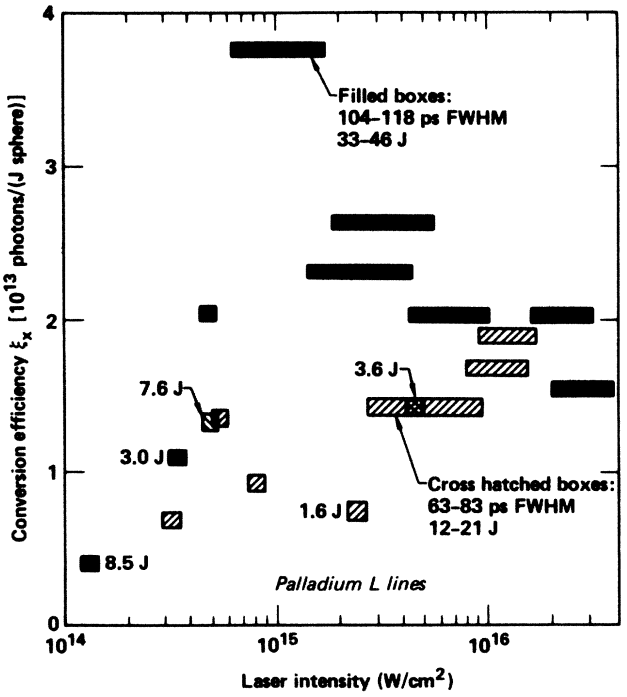

FIG. 2. Conversion efficiency vs laser intensity for the palladium $M \rightarrow L$ lines. The energy limits on the integration were typically 2.87—3.48 keV.

TABLE III. Summary of the $L \rightarrow K$ emission-band experiments at 0.53 μm.

Element	FWHM laser pulse width (ps)	Laser energy (J)	FWHM spot diam from the x-ray pinhole camera (μm)	Focal offset (μm)	Laser intensity (W/cm^2)	Conversion efficiency, ξ_x [photons/(joule sphere)]	X-ray FWHM (ps)
Chlorine	127	31.3	56	0	1.0×10^{16}	19×10^{11}	111
	109	33.1	99	-200	3.9×10^{15}	34×10^{11}	139
	125	35[a]	130	-360	2×10^{15}	55×10^{11}	122
	124	25.9	182	-580	8.0×10^{14}	105×10^{11}	126
	113	4.6	102	-360	5×10^{14}	50×10^{11}	77
	115	24.3	287	-920	3.3×10^{14}	77×10^{11}	98
	134	25.2	500	-1450	1.0×10^{14}	—	110
	125	24.9	500	-1450	1.0×10^{14}	27×10^{11}	82
Titanium	62	19.0	58 (sat.)	0	$1.5\text{-}2.9 \times 10^{16}$	5.2×10^{11}	48
	60	9.9	39	0	1.4×10^{16}	3.5×10^{11}	—
	57	19.1	61	-360	1.1×10^{16}	6.1×10^{11}	49
	59	19.0	76	-200	7.3×10^{15}	4.1×10^{11}	50
	54	17.4	139	-612	2.1×10^{15}	small	—
	117	34.8	64 (sat.)	-200	$>9.3 \times 10^{15}$	4.2×10^{11}	105
	~120	34.2	86 (sat.)	-200	$0.4\text{-}1.0 \times 10^{16}$	—	107
	~120	12.1	48	0	5.6×10^{15}	8.5×10^{11}	—
	144	29.3	89 (sat.)	-200	$3.1\text{-}7.2 \times 10^{15}$	—	117
	113	24.1	80	-200	4.2×10^{15}	3.5×10^{11}	106
	112	38.2	162	-580	1.7×10^{15}	12.2×10^{11}	112
	118	37.3	159	-360	1.6×10^{15}	11.8×10^{11}	120
	102	32.9	162	-360	1.6×10^{15}	13.0×10^{11}	115
	117	24.2	267	-810	3.7×10^{14}	5.7×10^{11}	80
Manganese	~70	12.3	37	0	1.6×10^{16}	1.0×10^{11}	57
	74	13.9	55 (sat.)	0	$0.9\text{-}1.8 \times 10^{16}$	1.6×10^{11}	56
	~70	10.3	37	0	1.4×10^{16}	1.2×10^{11}	—
	~70	11.8	96	-200	2.3×10^{15}	0.8×10^{11}	—
	122	34.5	63 (sat.)	0	$1.4\text{-}2.6 \times 10^{16}$	1.5×10^{11}	125
	110	37.1	64 (sat.)	-200	$>1.1 \times 10^{16}$	1.4×10^{11}	116
	127	31.2	156 (sat.)	-360	$1.1\text{-}3.4 \times 10^{15}$	3.1×10^{11}	127
	130	38.6	252	-580	6.0×10^{14}	3.4×10^{11}	121
	119	31.2	281	-810	4.2×10^{14}	1.2×10^{11}	98
Nickel	~550	35.9	123 (sat.)	—[b]	$0.6\text{-}6.0 \times 10^{15}$	2.5×10^{11}	350
	102	24.7	60 (sat.)	0	$1.2\text{-}2.3 \times 10^{16}$	—	97
	127	40.8	115 (sat.)	-200	$0.5\text{-}1.1 \times 10^{16}$	0.62×10^{11}	100
	107	28.9	80 (sat.)	0	$1.3\text{-}2.5 \times 10^{16}$	0.84×10^{11}	87
	104	28.2	82 (sat.)	0	$1.3\text{-}2.5 \times 10^{16}$	0.85×10^{11}	103
	103	40.6	95 (sat.)	-200	$0.6\text{-}1.4 \times 10^{16}$	0.80×10^{11}	97

[a] Laser energy was not measured because of computer failure; the value of 35 J is assumed because amplifiers were set to this value.
[b] Data omitted because of conflicting records.

aboloidal mirror. The target normal was at $\phi=0°,\theta=10°$ and the time-integrated spectrograph was at $\phi=28.8°,\theta=62.0°$, where θ is the polar angle from the paraboloidal mirror and ϕ is an azimuthal angle. The time-resolved spectrograph line of sight was between 62° and 72° to the target normal.

The conversion efficiencies ξ_x and x-ray pulse widths τ_x are given in Tables II and III. ξ_x is given in units of photons/(J sphere). We multiplied the measured $d\xi_x/d\Omega$ in photons/(J sr) by 4π sr to get ξ_x. The data are listed in order of decreasing intensity for each material with the 60-ps experiments listed first. The focal offset is the distance the target was moved away from the best focus position of the beam. The negative sign for the offsets means that the targets were always in the converging part of the $f/1.8$ laser beam. None of the x-ray pulse widths have been corrected for the 45-ps x-ray streak camera resolution, which was determined by the sweep rate and slit width. The laser pulse widths are accurate to about ± 10 ps for the pulse widths under 100 ps and to about $\pm 10\%$ for those over 100 ps. An uncertainty range of 1σ for the intensity is given whenever all the x-ray pinhole images for an experiment were exposed to a density exceeding the maximum density of 5.115 which could be measured by a microdensitometer. For each focal offset, the average full width at half maximum (FWHM) spot size and standard deviation were computed for the set of measurements for which good x-ray pinhole images were obtained. These were 44 ± 7, 75 ± 16, 130 ± 34, 223 ± 51, and 292 ± 26 μm for offsets of 0, -200, -360, -560 to -612, and -770 to -810 μm, respectively. It is these values that were used to generate the intensity ranges in the tables.

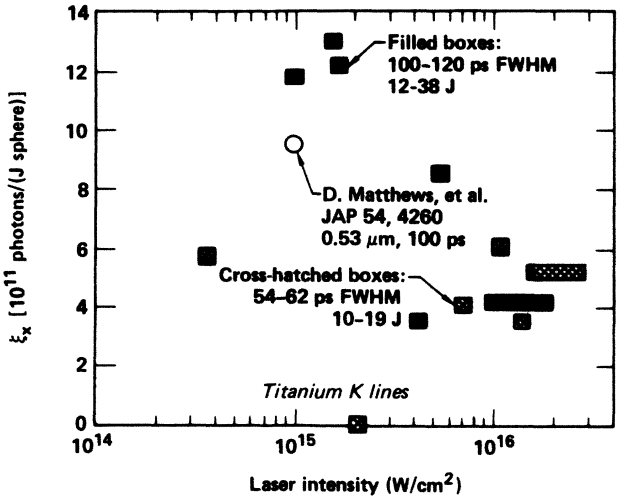

FIG. 3. Conversion efficiency vs laser intensity for the titanium $2p \rightarrow 1s$ lines for heliumlike and lithiumlike ions. The energy limits on the integration were typically 4.66—4.78 eV.

The chlorine, palladium, titanium, and manganese conversion efficiencies are plotted versus intensity in Figs. 1—4, respectively. All four curves at 120 ps show the conversion efficiency peaking at an intermediate intensity. The absorption fractions, which were not measured, may have been higher at lower intensities. The longer scale lengths over which the heat has to be transported at the higher intensities may also partly explain this peak.

We studied the $M \rightarrow L$ emission bands for several elements, ranging in Z from 39 (Y, 2.00—2.36 keV) to 68 (Er, 7.1—8.25 keV). The total integrated brightnesses of the low-energy L lines are considerably brighter than K lines at near the same energies. At higher x-ray energies, only the K lines can be generated. The highest energy $M \rightarrow L$ lines which we observed were from cesium (Table II). The Ne-like $M \rightarrow L$ lines, which were strong for Y and Pd, were absent for cesium even at high intensity. We looked for the erbium $M \rightarrow L$ lines, which we expected to be in the energy range 7.1—8.25 keV, but saw only the continuum emission.

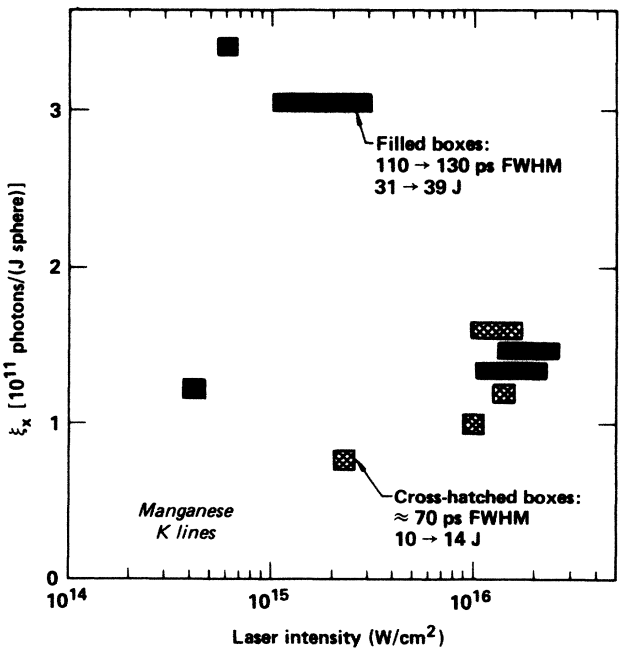

FIG. 4. Conversion efficiency vs laser intensity for the manganese $2p \rightarrow 1s$ lines for heliumlike and lithiumlike ions. The energy limits on the integral ion were typically 6.02—6.25 keV.

At high x-ray energies, the lines from an $L \rightarrow K$ emitter are brighter than those from an $M \rightarrow L$ emitter. To see why this is so, neglect screening and use the simple nonrelativistic hydrogenic energy levels. It then takes $\frac{4}{5}$ of the $M \rightarrow L$ transition energy to remove the last M-shell electron while it takes only $\frac{1}{3}$ of the $L \rightarrow K$ transition energy to remove the last L-shell electron.

III. DISCUSSION

The $2p \rightarrow 1s$ lines we observed were primarily from heliumlike and lithiumlike ions. The $K\alpha$ line was always comparatively weak. Representative $L \rightarrow K$ spectra from Cl, Ti, and Mn experiments and $M \rightarrow L$ spectra from Y, Pd, and Cs experiments are shown in Figs. 5 and 6, respectively. Neonlike $M \rightarrow L$ line energies were calculated using Mosely fits to the experimental results of Burkhalter *et al.*[3] and then identified in our spectra to get the energy scale in Fig. 6. Similarly, $2p \rightarrow 1s$ transition energies were obtained from Scofield's calculations[4] and then used to identify lines to fix the energy scale for Fig. 5. We selected the shots with the highest conversion efficiency at 120 ps for the chlorine and nickel spectra and at 60 ps for the palladium, titanium, and manganese spectra. The chlorine $^3P_1$ and $^1P_1$ $1s2p \rightarrow 1s^2\,{}^1S_0$ lines are flat topped since their film density exceeded the maximum density of 5.115 which could be microdensitometered.

Table IV gives the ratios of the area under several lines involving a $2p \rightarrow 1s$ transition to the area under the $1s2p\,{}^1P_1 \rightarrow 1s^2\,{}^1S_0$ line. The $K\alpha$ line is more intense at 60 ps than at 120 ps for both titanium and manganese. This is expected since the superthermal electrons will not have so far to diffuse to reach cold material for the shorter laser pulse length. The letter designations for the satellite $L \rightarrow K$ lines are taken from Gabriel.[5] The e, j, k, and l lines are in the $1s2p^2 \rightarrow 1s^2 2p$ array of lines, and the q and r lines are in the $1s2s2p \rightarrow 1s^2 2s$ array.

X-ray flashes that are both short and bright can only be achieved over a finite wavelength or energy range. At low x-ray photon energy, the problem in producing a short x-ray flash is that recombination may take too long, resulting in a tail that persists long after the laser pulse. At high energy, the problem is that there must be sufficient time for the atoms to strip down to the required electron configuration. We will now estimate the rates for collisional ionization and three-body recombination in order to show that our experimental results are reasonable.

First we find a lower limit for the collisional ionization time τ_{iK}. Assume that the maximum electron density at which the x-ray line generation can occur is at most a few times the critical density for the laser frequency. Having

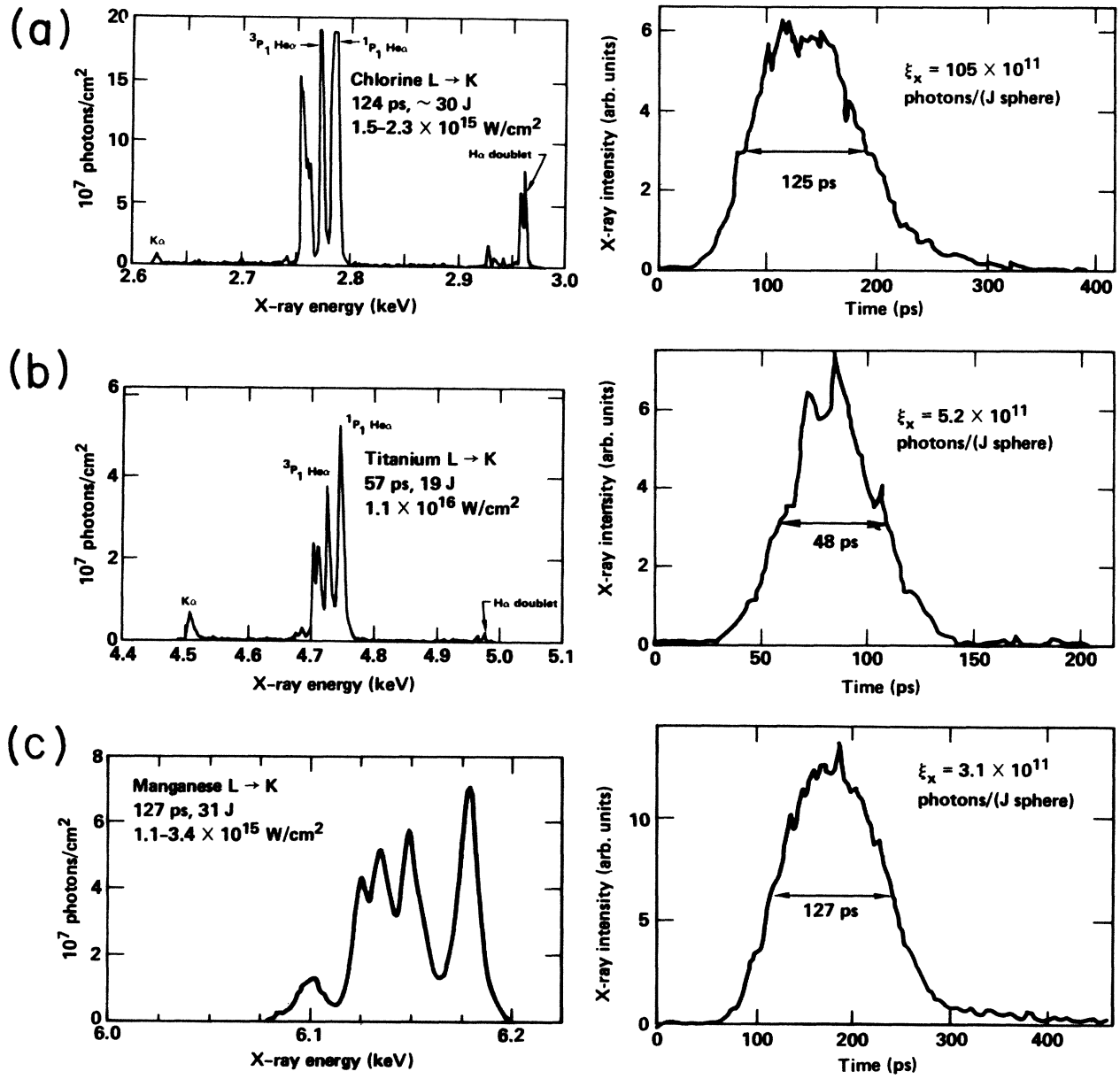

FIG. 5. Spectrum and time history of the $2p \rightarrow 1s$ line emission for several elements. (a) Chlorine: 8×10^{14} W/cm^2, 124 ps, 25.9 J, $\xi_x=105\times10^{11}$ photons/(J sphere), and $\tau_x=126$ ps. (b) Titanium: 1.1×10^{16} W/cm^2, 57 ps, 19.1 J, $\xi_x=6.1\times10^{11}$ photons/(J sphere), and $\tau_x=49$ ps. (c) Manganese: $(1.1-3.4)\times10^{15}$ W/cm^2, 127 ps, 31.2 J, $\xi_x=3.1\times10^{11}$ photons/(J sphere), and $\tau_x=127$ ps.

fixed n_e, there is a T_e which minimizes τ_{iK}. Using Seaton's[6] result for the near-threshold collisional ionization cross section, the collisional ionization time τ_{ik} can be calculated to be

$$\frac{1}{\tau_{iK}}=\frac{256\sqrt{\pi}}{9n}\bar{g}a_0^2\alpha c n_e\left[\frac{E_H}{I}\right]^{3/2}\times\left[\left[\frac{I}{kT}\right]^{1/2}E_2\left[\frac{I}{kT}\right]\right]. \quad (1)$$

The exponential integral $E_2(x)$ is given by

$$E_2(x)=\int_1^\infty \frac{e^{-xt}}{t^2}dt\ . \quad (2)$$

The factor in square brackets in Eq. (1) has the limits

$$[\cdots]_{\overrightarrow{kT\ll I}}\left[\frac{kT}{I}\right]^{1/2}\exp\left[\frac{-I}{kT}\right], \quad (3a)$$

$$[\cdots]_{\overrightarrow{kT\gg I}}\left[\frac{I}{kT}\right]^{1/2}. \quad (3b)$$

The factor in square brackets in Eq. (1) carries all the

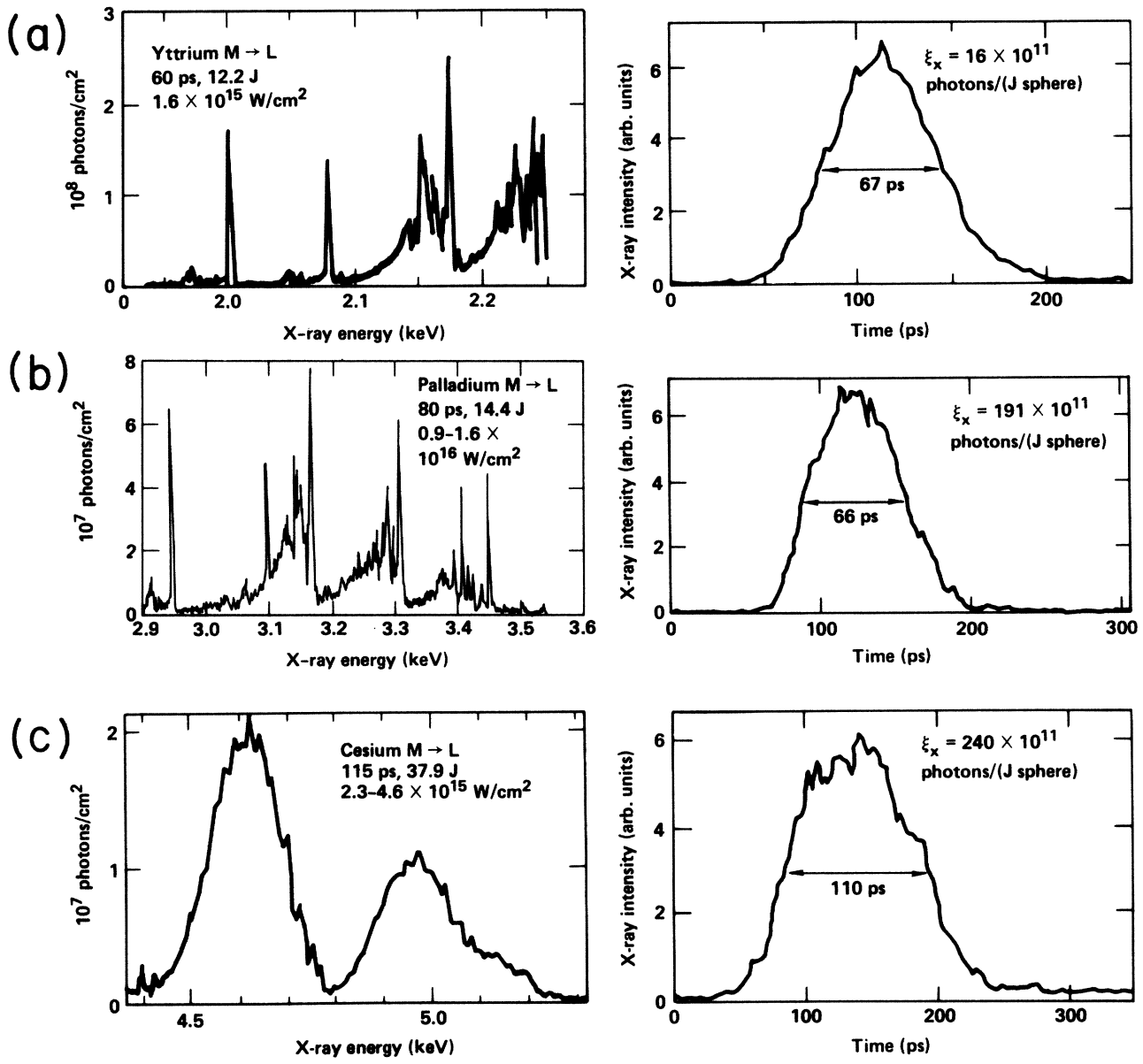

FIG. 6. Spectrum and time history of the $M \rightarrow L$ line emission for several elements. (a) Yttrium: 1.6×10^{15} W/cm^2, $\sim$60 ps, 12.2 J, $\xi_x=2.4\times10^{13}$ photons/(J sphere), and $\tau_x=67$ ps. (b) Palladium: $(0.6-1.6)\times10^{15}$ W/cm^2, 108 ps, 39.6 J, $\xi_x=378\times10^{11}$ photons/(J sphere), and $\tau_x=157$ ps. (c) Cesium: $(2.3-4.6)\times10^{15}$ W/cm^2, 115 ps, 37.9 J, $\xi_x=16\times10^{11}$ photons/(J sphere), and $\tau_x=110$ ps.

temperature dependence of τ_{iK}. It has a maximum value of 0.2541 at $kT=3.75I$. Here a_0 is the Bohr radius of 0.529 Å, E_H is the hydrogen ionization energy of 13.61 eV, c is light speed, α is the dimensionless electromagnetic fine-structure constant of 1/137.036, n_e is the density of free electrons, and n is the Rydberg shell number. The $\bar{g}$ is the Gaunt factor for photoionization, which we take to be about 0.42.

Let us look at the 7.804-keV nickel $1s2p\ ^1P_1 \rightarrow 1s^2\ ^1S_0$ line, for example. The energy required to strip nickel from $2s\ 1s^2$ to $1s^2$ is 2398 eV.[7] Thus,

$$(\tau_{iK})_{\min}=(141\text{ ps})\left[\frac{10^{21}\text{ cm}^{-3}}{n_e}\right]. \quad (4)$$

The critical density for 1.064-μm light is 0.985×10^{21} electrons/cm^3. To completely strip the L shell requires a time on the order of ln(8/0.5) times τ_{iK}, since the population of eight electrons in the L shell decreases exponentially with the time constant τ_{iK}. At least 400 ps is actually required to strip the nickel for a free-electron density of $n_e=10^{21}$ cm^{-3}. Flash radiography at <100 ps and

TABLE IV. Chlorine, titanium, and manganese line ratios.

Element	Intensity (W/cm^2)	Laser FWHM pulse width (ps)	Kα / $^1P_1$ Heα	Li-Like[a] jkl, qr, e / $^1P_1$ Heα	$^3P_1$ Heα / $^1P_1$ Heα	Hα doublet / $^1P_1$ Heα
Chlorine	1.0×10^{16}	127	—	0.34	0.30	0.46
	3.9×10^{15}	109	—	0.29	0.20	0.20
	$\sim 1.7 \times 10^{15}$	125	0.005	0.34	0.19	0.10
	8.0×10^{14}	124	0.008	0.39	0.42	0.07
	5×10^{14}	113	—	0.34	0.30	0.00
	3.3×10^{14}	115	0.014	0.57	0.42	0.00
	1.0×10^{14}	125	—	0.58	—	0.00
Titanium	$\sim 10^{16}$	117	0.02	0.61	0.55	0.015
	5.6×10^{15}	120	0.02	0.60	0.54	0.00
	4.2×10^{15}	113	0.05	0.82	0.66	0.00
	3.7×10^{14}	117	0.04	1.37	0.69	0.00
	$(1.5\text{-}2.9) \times 10^{16}$	62	0.23	0.73	0.52	0.027
	1.4×10^{16}	60	0.13	0.72	0.60	0.025
	1.1×10^{16}	57	0.21	0.78	0.55	0.025
	7.3×10^{15}	59	0.17	0.65	0.59	<0.02
Manganese	$(1.4\text{-}2.6) \times 10^{16}$	122	0.056	0.78	<0.63	—
	$>1.1 \times 10^{16}$	110	0.00	0.80	<0.61	—
	$(1.1\text{-}3.4) \times 10^{15}$	127	0.00	1.42	—	—
	6.0×10^{14}	130	0.00	2.01	—	—
	4.2×10^{14}	119	0.00	3.40	—	—
	1.6×10^{16}	~70	0.41	0.88	<0.70	—
	$(0.9\text{-}1.8) \times 10^{16}$	~74	0.41	0.83	<0.55	—
	1.4×10^{16}	~70	0.68	1.10	<0.63	—
	2.3×10^{15}	70	1.03	1.27	<0.65	—

[a] Notation from A. H. Gabriel, Mon. Not. R. Astron. Soc. **160**, 99 (1972), Table V.

1.064 μm using the nickel Heα lines is thus not expected to be possible, and is expected to be but barely possible for 0.53 μm.

The three-body recombination rate into a Rydberg shell can be derived either indirectly from detailed balance with collisional ionization or directly by considering classical electron-electron collisions in the Coulomb field of an ion and using the Bohr model.[8] In particular, detailed balance with collisional ionization using the Thomson formula[9] for the collisional ionization cross section gives

$$\frac{1}{\tau_{3R}} = 192\pi^2 \alpha f n_e^2 a_0^5 c \frac{n^4}{Z^2} \left[\frac{E_H}{kT}\right]^2 \times \left[\int_0^\infty \frac{1}{(t+1)^2} e^{-(E_b/kT)t}\, dt\right]. \quad (5)$$

Here $f = \frac{1}{3}$ if Thomson's classical cross section is used for the collisional ionization. The result of evaluating $192\pi^2\alpha/3$ is 4.61. If n is not too high, then radiative decay down to the ground state is rapid. For high n, the problem is much more complex. Low-momentum-transfer collisions will transfer electrons in high-n states preferentially to near-neighbor-n states. Mathematically, it looks like diffusion, as discussed by Zel'dovich and Raizer.[10]

For simplicity, we will consider only those n states for which radiative decay is rapid. This will give us a lower limit to the three-body recombination rate. We have

$$\tau_{3R} = (83 \text{ ps}) \left[\frac{T}{1 \text{ keV}}\right]^2 \left[\frac{10^{22} \text{ cm}^{-3}}{n_e}\right]^2 Z^2 \Big/ \sum_{n=1}^{n_{\max}} n^4 . \quad (6)$$

We need to know what to use as $n_{\max}$. Bethe and Heitler[11] give the summed oscillator strengths $F_{n'n} \equiv \Sigma_{l,l',m,m'} f_{nlm}^{n'l'm}$ for the spontaneous transition rate for hydrogen from the Rydberg shell n to the lower n'. The spontaneous Einstein A_E coefficient is then $A_E = (F_{n'n}/n^2) k^2 r_0 c$, or

$$(A_E)_{n \to n'} = \frac{1}{n^2} \left[\frac{2^6}{3\sqrt{3}\pi} \left[\frac{1}{n'^2} - \frac{1}{n^2}\right]^{-3} \frac{1}{n^3} \frac{1}{n'^3}\right] k^2 r_0 c . \quad (7)$$

This rate is averaged over all possible l,m values for shell n and summed over all possible l',m' values for shell n'. It is an approximate result for nonrelativistic, hydrogenic ions. Here k is the wave number of the emitted photon, $r_0 = 2.818 \times 10^{-13}$ cm is the classical electron radius, and c is the speed of light. We have divided the $F_{n'n}$ by n^2 to get an averaged rather than a summed oscillator strength for the upper shell n. The wave number k equals $(Z^2 E_H/\hbar c)[(1/n')^2 - (1/n)^2]$, where E_H is the hydrogenic ionization energy of 13.6 eV and Z is the effective charge of ion, taking into account screening by the other electrons.

A measure of the rate of the radiative cascade to lower levels is given by

$$\frac{d}{dt}\left\langle\frac{1}{n^2}\right\rangle=\sum_{n'=1}^{n-1}\left[\frac{1}{n'^2}-\frac{1}{n^2}\right](A_E)_{n\to n'}$$

$$\cong\frac{1}{(53\text{ ps})n^5/\bar{Z}^4}\ . \tag{8}$$

Let $n_{\max}$ be that value of n for which the right-hand side of Eq. (8) equals τ_{3R}^{-1}. Substituting that value for $n_{\max}$ into Eq. (6), we obtain the three-body recombination rate as limited by spontaneous radiative decay:

$$\tau_{3R}^{-1}=0.07\left[\frac{1\text{ keV}}{T}\right]\left[\frac{n_e}{10^{22}\text{ cm}^{-3}}\right]\bar{Z}\text{ ps}^{-1}\ . \tag{9}$$

Line emission can persist after the laser pulse only if either the electron temperature stays high for a time or if highly stripped ions are created which take a long time to recombine. The hydrodynamic cooling time should be comparable to the laser pulse width for one-dimensional expansion or possibly even much shorter for three-dimensional expansion. A significant tail to an x-ray flash was observed only for the chlorine $1s2p\to 1s^2$ lines. Chlorine also had strong $H\,\alpha$ emission. Hydrogenic ions were probably recombining slowly in the low-density plasma. If no hydrogenic ions are created and if the temperature drops rapidly, then there can be no $1s2p\to 1s^2$ emission after the laser pulse.

IV. TWO-PARAMETER TRANSFORMATION GROUP FOR THE HYDRODYNAMIC EQUATIONS

We can show, from very general arguments, just how shorter-wavelength irradiance is better for flash radiography. We will derive scaling relations from the hydrodynamic equations which include either flux-limited or classical heat conduction and which include the deposition of the laser beam energy into the plasma. The conservation equations for mass, momentum, and energy in one dimension are

$$\frac{\partial\rho}{\partial t}+\frac{\partial}{\partial x}(\rho u)=0\ , \tag{10}$$

$$\frac{\partial}{\partial t}(\rho u)+\frac{\partial}{\partial x}(p+\rho u^2)=0\ , \tag{11}$$

$$\frac{\partial}{\partial t}\left[\rho\left[\varepsilon+\frac{u^2}{2}\right]\right]+\frac{\partial}{\partial x}\left[\rho u\left[\varepsilon+\frac{u^2}{2}\right]+pu+J\right]=P(x,t)\ . \tag{12}$$

Here t and x are time and distance, ρ is density, u is the matter velocity, p is pressure, ε is the internal energy per gram, J is the heat flux in ergs/(cm^2 sec), and $P(x,t)$ is the laser beam energy deposited per unit volume and per unit time. We assume $P(x,t)$ has the form

$$P(x,t)=I(t)f(\rho(x,t))\frac{\partial\rho(x,t)}{\partial x}\ . \tag{13}$$

The function f is normalized so that $\int f(\rho)d\rho=1$. Thus $I(t)$ is the incident laser intensity, and $f(\rho)d\rho$ is the fraction of the laser energy that is deposited in the density interval $\rho-\frac{1}{2}d\rho$ to $\rho+\frac{1}{2}d\rho$. The heat flux J has one of the forms

$$J=\begin{cases}\pm f\left[\dfrac{kT_e}{m_e}\right]^{1/2}kT_en_e & \text{flux limited}\ ,\\ -\frac{2}{7}\lambda_c'\dfrac{\partial}{\partial x}T_e^{7/2} & \text{classical}\ .\end{cases} \tag{14}$$

Here, f is the flux limiter, a dimensionless number usually taken to be between 0.03 and 0.1, and λ_c' is a constant which is independent of both the density and temperature.

The internal energy per gram ε is assumed to be proportional to temperature. The pressure is assumed proportional to the product of the density and the temperature. The effects of radiation cooling and radiative heat transport are neglected.

We find three-parameter scaling groups both for the case of purely classical heat conduction and for the case of purely flux-limited heat conduction. This latter case is, however, highly unphysical. The heat flow cannot be everywhere flux limited. The case of purely classical heat conduction is of interest only for short laser wavelength and low intensity. Usually, the heat flow is flux limited, but only in certain regions and at certain times. Fortunately, there is a two-parameter scaling group which applies regardless of whether the heat flow is classical, flux limited, or partially both. We now give these transformation groups.

For flux-limited heat conduction, if $\rho(x,t)$, $u(x,t)$, $T(x,t)$, $I(t)$, and $f(\rho)$ comprise a solution set, then so do

$$\begin{aligned}&\rho_A(x,t)=A\rho(x,t),\quad u_A(x,t)=u(x,t)\ ,\\ &T_A(x,t)=T(x,t)\ ,\\ &I_A(t)=AI(t)\ ,\quad f_A(\rho_A)=A^{-1}f(A^{-1}\rho_A)\end{aligned} \tag{15}$$

and

$$\begin{aligned}&\rho_B(x,t)=\rho(x,\sqrt{B}t)\ ,\quad u_B(x,t)=\sqrt{B}u(x,\sqrt{B}t)\ ,\\ &T_B(x,t)=BT(x,\sqrt{B}t)\ ,\\ &I_B(t)=B^{3/2}I(\sqrt{B}t)\ ,\quad f_B(\rho_B)=f(\rho_B)\end{aligned} \tag{16}$$

and

$$\begin{aligned}&\rho_C(x,t)=\rho(Cx,Ct)\ ,\quad u_C(x,t)=u(Cx,Ct)\ ,\\ &T_C(x,t)=T(Cx,Ct)\ ,\\ &I_C(t)=I(Ct)\ ,\quad f_C(\rho_C)=f(\rho_C)\ .\end{aligned} \tag{17}$$

For classical heat conduction, the alternate solutions are

$$\begin{aligned}&\rho_A(x,t)=A\rho(Ax,At)\ ,\quad u_A(x,t)=u(Ax,At)\ ,\\ &T_A(x,t)=T(Ax,At)\ ,\\ &I_A(t)=AI(At)\ ,\quad f_A(\rho_A)=A^{-1}f(A^{-1}\rho_A)\end{aligned} \tag{18}$$

and

$$\rho_B(x,t)=B\rho(x,B^{1/4}t),\quad u_B(x,t)=B^{1/4}u(x,B^{1/4}t),$$
$$T_B(x,t)=\sqrt{B}\,T(x,B^{1/4}t)\,, \tag{19}$$
$$I_B(t)=B^{7/4}I(B^{1/4}t),\quad f_B(\rho_B)=B^{-1}f(B^{-1}\rho_B)$$

and

$$\rho_C(x,t)=C\rho(x/C,t/\sqrt{C}),\quad u_C(x,t)=\sqrt{C}\,u(x/C,t/\sqrt{C})\,,$$
$$T_C(x,t)=CT(x/C,t/\sqrt{C})\,, \tag{20}$$
$$I_C(t)=C^{5/2}I(t/\sqrt{C}),\quad f_C(\rho_C)=C^{-1}f(C^{-1}\rho_C)\,.$$

For flux-limited heat transport, solution A tells us what happens if the laser wavelength is changed so that the absorption takes place at A times the original density. The laser intensity must be increased by the same factor A to maintain the same electron temperature profile, only now the density for each temperature is A times as great. We are heating up A times as much matter at A times the density. Solution C tells us that if we shorten the pulse, the length and time scales for the hydrodynamic variables shorten correspondingly. Except for this change of scale, the hydrodynamic variables have the same shapes and the same peak values.

For classical heat conduction, it is again solution A which tells what happens if the laser wavelength is changed so that the absorption is at A time the original density. Both the length and time scales are shrunk. With a laser pulse at $1/\sqrt{A}$ times the original wavelength, A times the original intensity, and $1/A$ times the original pulse width, we heat up the same amount of matter as before, but at A times the density.

The two-parameter scaling group is given by

$$\rho_{(A,B)}(x,t)=A\rho\left[\frac{x}{AB^2},\frac{t}{\sqrt{A}B^{3/2}}\right],$$
$$u_{(A,B)}(x,t)=\sqrt{AB}\,u\left[\frac{x}{AB^2},\frac{t}{\sqrt{A}B^{3/2}}\right],$$
$$T_{(A,B)}(x,t)=ABT\left[\frac{x}{AB^2},\frac{t}{\sqrt{A}B^{3/2}}\right], \tag{21}$$
$$f_{(A,B)}(\rho_{(A,B)})=A^{-1}f(A^{-1}\rho_{(A,B)})\,,$$

and

$$I_{(A,B)}(t)=A^{5/2}B^{3/2}I\left[\frac{t}{\sqrt{A}B^{3/2}}\right].$$

We do not have the freedom we had previously to independently change the density where the absorption occurs, the laser intensity, and the laser pulse width. Only two of these three quantities may now be specified. We then obtain a new solution for the hydrodynamic variables.

This scaling predicts that if we observe a line conversion efficiency ξ_x at intensity I_1, laser pulse length τ_1, and laser wavelength λ_1, then at wavelength $\lambda_2<\lambda_1$, intensity $I_2=I_1\lambda_1^2/\lambda_2^2$, and pulselength $\tau_2=\tau_1\lambda_2^2/\lambda_1^2$, the x-ray line conversion efficiency ξ_x should be unchanged. There are a number of important invariants in this scaling. The scaling is obtained by letting $A=\lambda_1^2/\lambda_2^2$ and letting $B=A^{-1}$. The distance and time scales are shortened by the factor λ_2^2/λ_1^2, while the density scale is increased by the factor λ_1^2/λ_2^2. The Lagrangian mass coordinate $m=\int\rho\,dx$ is unchanged. Fluid elements at the same Lagrangian mass coordinate are unchanged in temperature and velocity. Since $I\lambda^2$ has not changed, resonance absorption produces the same distribution of superthermal electrons which deposit their energy in the same way since the Lagrangian mass coordinates are unchanged. The amount and details of the inverse bremsstrahlung are preserved since, although the inverse bremsstrahlung absorption coefficient is a factor of λ_1^2/λ_2^2 greater due to the higher density, the distance scale has been correspondingly shortened. Even though less time is available for stripping the ions, the increased density exactly compensates, assuming that electron collisions and not photoionizations are predominant. Both $\rho\tau$ and $\rho L/u$ are invariants. L/u is a measure of the time the ion spends in the hot, dense region where the line generations occurs before it is convected into the corona.

There are physical processes which have not been considered whose qualitative effects are known. First, L/λ is not invariant, but rather is proportional to λ. At the shorter wavelength, fewer wavelengths of plasma are present for Brillouin scattering. Also, three-body recombination occurs more efficiently at the shorter wavelength, since $\rho^2\tau$ is proportional to λ^{-2}. If, at the longer wavelength, the x-ray line emission persists due to incomplete recombination before the ions are convected into the corona, the level of this tail will be less at the shorter wavelength and it will go away relatively faster. If the heat flow is limited by ion turbulence, it will likely be less so at the shorter wavelength and higher density since ν_{eff} is proportional to the electron plasma frequency ω_{pe} or to $\sqrt{\rho}$, whereas ν_{ei} is proportional to the ion density or to ρ. Thus, at the shorter wavelength, densities further above the critical electron density may be heated, thus increasing the x-ray line emission.

Thus, for those conditions for which we observed bright 50-ps x-ray flashes for 2ω irradiation, we would expect to be able to achieve, using 4ω irradiation, x-ray flashes four times shorter and four times more intense but with the same time-integrated x-ray emission per unit area on the source. Of course, the irradiance at 4ω would have to be four times as intense and last but one-fourth as long.

V. CONCLUSION

Bright x-ray flashes of duration 50 ps or less have been demonstrated for the Y $M\rightarrow L$ lines (2.00—2.35 keV), Pd $M\rightarrow L$ lines (2.95—3.46 keV), and Ti $L\rightarrow K$ lines (4.75 keV $1s2p\ ^1P_1\rightarrow 1s^2\ ^1S_0$). Based upon the two-parameter transformation group, there is reason to believe that bright 10—20 ps flashes at these same energies should be possible with 4ω irradiation.

ACKNOWLEDGMENTS

Dave Sullivan and John Brundage, together with many other employees of KMS Fusion, Inc., helped us to con-

TABLE V. Crystal and film calibrations for the time-integrated spectrograph.

Spectrograph center energy (keV)	Crystal	R_c (radians)	Assumed Kodak Direct Exposure film calibration (photons/cm^2)
2.1	(002) PET	1.12×10^{-4}	$4.9\times10^{7}\,D_{0.1\text{ N.A.}}\times(1+0.0131D^{3}_{0.1\text{ N.A.}})$
2.8	(111) Si	5.4×10^{-5}	$4.4\times10^{7}D_{0.1\text{ N.A.}}\times(1+0.0169D^{3}_{0.1\text{ N.A.}})$
3.2	(111) Si	4.65×10^{-5}	$4.67\times10^{7}\,D_{0.1\text{ N.A.}}\times(1-0.106D_{0.1\text{ N.A.}}+0.031D^{2}_{0.1\text{ N.A.}})$
4.75	(200) LiF	1.5×10^{-4}	$3.37\times10^{7}\,D^{0.87}_{\text{diffuse}}\times(1+0.11D_{\text{diffuse}})$
6.2	(200) LiF	2.1×10^{-4}	$4.03\times10^{7}\,D^{0.87}_{\text{diffuse}}\times(1+0.084D_{\text{diffuse}})$
7.8	(200) LiF	2.34×10^{-4}	$4.84\times10^{7}\,D^{0.87}_{\text{diffuse}}\times(1+0.07D_{\text{diffuse}})$

duct these experiments. We thank Gary Stone, Vicki Martin, and Betty Stewart for digitizing the film. This work was performed under the auspices of the U.S. Department of Energy by the Lawrence Livermore National Laboratory under Contract No. W-7405-ENG-48.

APPENDIX: DIAGNOSTICS

The x-ray diffraction crystals used in the time-integrated spectrograph were calibrated at KMS Fusion, Inc. Table V gives the angle-integrated reflectivities R_c and the Kodak Direct Exposure film (DEF) calibrations for the various x-ray lines which were observed. The film was measured by a microdensitometer with a 10× objective lens which had matching input and output numerical aperatures (N.A.) of 0.25. The calibrations for the Ti, Mn, and Ni Heα lines are obtained directly from the measurements of Rockett *et al.*,[12] and are in terms of the diffuse density. The diffuse density is first converted to specular density for 0.1 N.A. optics and then to specular density for 0.25 N.A. optics. Conversion from D(diffuse) to D(0.1 N.A.) was made using a fit to Fig. 6 in their paper. The conversion from D(0.1 N.A.) to D(0.25 N.A.) was done on the basis of measurements made by G. Stone at Lawrence Livermore National Laboratory. The film calibrations at 2.1, 2.8, and 3.2 keV were provided by P. Burkhalter at the Naval Research Laboratory and assume a 0.1 N.A. Again, we had to convert to 0.25 N.A. specular density values.

The conversions used are

$$\begin{aligned} D(\text{diffuse}) &= [0.478+0.0236D(0.1\text{ N.A.})] \\ &\quad\times D(0.1\text{ N.A.}), \\ D(0.08\text{ N.A.}) &= [1.28-0.077D(0.25\text{ N.A.})] \\ &\quad\times D(0.25\text{ N.A.}). \end{aligned} \tag{22}$$

Assuming $D(0.08\text{ N.A.})\approx D(0.1\text{ N.A.})$ gives

$$D(\text{diffuse}) = 0.61D(0.25\text{ N.A.}). \tag{23}$$

All densities have had the density of the unexposed film subtracted.

The (200) LiF and (111) Si crystals were calibrated at the Ti $K\alpha,K_\beta$, and Cl $K\alpha$ lines, respectively. The results were scaled to the appropriate energies using the $R_c(\theta)$ curves of Gilfrich, Brown, and Burkhalter[13] for (200) LiF, and using the $R_c(\theta)$ curve of Burek[14] for (111) Si. Burek's double-crystal data was converted to single-crystal reflectivity after scaling by assuming a perfect crystal with zero absorption. The (002) pentaerythritol (PET) crystal was not calibrated. The R_c value of 1.12×10^{-4} rad is simply a value taken from Gilfrich *et al.*[13]

A Ken Tech streak camera, with a cesium-iodide photocathode and a 0.75-mm-wide slit was used. The streak speed was measured to be 27 ps/mm by irradiating a brass wire with a train of five 110-ps FWHM laser pulses separated by 218±4 ps. The timing was also checked by simply changing the cable delay 420 ps, giving 28 ps/mm. The camera was operated at the no. 4 sweep setting for all these experiments. The magnification was measured to be 2.27 by taping a washer over the slit. Within several percent, this is what magnification is needed to match the calculated spectral line positions at the photocathode. The slit width of 0.75 mm represents a time resolution of 45 ps. None of the FWHM x-ray pulsewidths in the tables have been corrected for this time resolution. Many of the x-ray pulsewidths for the 60-ps experiments are near the 45-ps time resolution and must actually be considerably shorter. The Ken Tech streak camera for the time-resolved spectrograph was located at $\phi=-45°$, $\theta=90°$.

An x-ray pinhole camera at $\phi=0°$, $\theta=52°$ took four images with magnification 7.1. All four pinholes were 17 μm in diameter and were filtered with 2.5 mils of beryllium. The target-to-pinhole distances was 5.5 cm.

[1]B. Yaakobi, P. Bourke, Y. Conturie, J. Dellettrez, J. M. Forsyth, R. D. Frankel, L. M. Goldman, R. L. McCrory, W. Seke, J. M. Soures, A. J. Burek, and R. E. Deslattes, Opt. Commun. **38**, 196 (1981).

[2]D. L. Matthews, E. M. Campbell, N. M. Ceglio, G. Hermes, R. Kauffman, L. Koppel, R. Lee, K. Manes, V. Rupert, V. W. Slivinsky, R. Turner, and F. Ze, J. Appl. Phys. **54**, 4260 (1983).

[3]P. G. Burkhalter, D. J. Nagel, and R. Cowan, Phys. Rev. A **11**, 782 (1975).

[4]J. H. Scofield, Lawrence Livermore National Laboratory, Report No. UCID-16848, 1975 (unpublished).

[5]A. H. Gabriel, Mon. Not. R. Astron. Soc. **160**, 99 (1972).

[6]M. J. Seaton, in *Atomic and Molecular Processes,* edited by D. R. Bates (Academic, New York, 1962), p. 416.

[7]C. W. Allen, *Astrophysical Quantities,* 3rd ed. (University of London, The Athlone Press, London, 1973), p. 38.

[8]D. W. Phillion and C. J. Hailey, Lawrence Livermore National Laboratory, Livermore, California 94550, Report No. UCRL-94206 (unpublished).

[9]Dimitri Mihalas, *Stellar Atmospheres,* 2nd ed. (Freeman, San Francisco, 1978), p. 124.

[10]Ya. B. Zel'dovich and Yu. P. Raizer, *Physics of Shock Waves and High-Temperature Hydrodynamic Phenomena* (Academic, New York, 1966), Vol. I. p. 408.

[11]H. A. Bethe and E. E. Salpeter, *Quantum Mechanics of One and Two Electron Atoms* (Springer-Verlag, Berlin, 1957), p. 269.

[12]P. Rockett, C. R. Bird, C. J. Hailey, D. Sullivan, and P. G. Burkhalter, Appl. Opt. **24**, 2536 (1985).

[13]J. V. Gilfrich, D. B. Brown, and P. G. Burkhalter, Appl. Spectrosc. **29**, 322 (1975).

[14]Anthony Burek, Space Sci. Rev. **53**, (1976).